

Sensors for carbon monoxide based on Pd/SnO₂/CNT nanocomposites

Qinghua Hu¹, Shantang Liu^{*1}, and Yongfu Lian^{**2}

¹ School of Chemistry and Environmental Engineering, Wuhan Institute of Technology, Xiongchu Avenue 693, Wuhan 430074, P.R. China

² Key Laboratory of Functional Material Chemistry, Ministry of Education, School of Chemistry and Materials Science, Heilongjiang University, Harbin 150080, P.R. China

Received 29 May 2014, revised 18 July 2014, accepted 23 July 2014

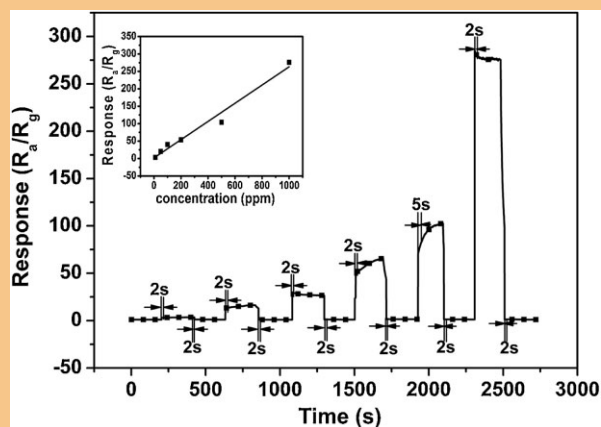
Published online 25 August 2014

Keywords carbon nanotubes, CO, doping, gas sensors, nanoparticles, SnO₂

* Corresponding author: e-mail liushantang@mail.wit.edu.cn, Phone: +27-87195001(o), Fax: +27-87195001

** e-mail chyflian@hlju.edu.cn, Phone: +86 451 86608516, Fax: +86 451 86608516

This study investigates using a Pd²⁺-doped Pd/SnO₂/CNT nanocomposite (Pd²⁺/SnO₂/CNT) sensor to detect carbon monoxide (CO). Using a simple, controllable sol-gel method, we synthesized a CNT that was coated by Pd²⁺-doped SnO₂ nanoparticles. The prepared materials are highly sensitive to CO at a low temperature and demonstrate a fast response-recovery time. The hybrid Pd²⁺/SnO₂/CNT sensors exhibit high sensitivity, selectivity, repeatability, a low limit of detection (5 ppm, $R_a/R_g = 1.95$), and a fast response-recovery ($t_{90} \leq 2$ s) to CO at 100 °C. The sensitivity of the materials was improved to 80 times higher than pure tin oxide at a CO concentration of 500 ppm. Such behaviors may be attributed to the catalytic activity of the PdO nanoparticles, the active reaction site that was generated by the CNT, and the enhanced chemisorption and dissociation of the gas.



© 2014 WILEY-VCH Verlag GmbH & Co. KGaA, Weinheim

1 Introduction Extensively used in various field, rutile-structured tin oxide (SnO₂ and impurity doped SnO₂) is an n-type semiconducting material [1]. It is regarded to be an important functional material, due to its advantageous properties, including its high sensitivity, high stability, fast response, and low cost [2, 3]. It has three major applications: (1) as a transparent conducting oxide (TCO); (2) as an oxidation catalyst; and (3) as a solid state gas sensing material [4].

Researchers have developed various methods for preparing SnO₂, including microwave-induced combustion [5], a hydrothermal process [6], a spray pyrolysis [7], a chemical vapor deposition [8], and a sol-gel method [9]. As a simple and controllable method, the sol-gel method achieves high purity, superfine particles.

The main performance parameters of a sensor are its response time, recovery time, optimum working temperature, and a low limit of detection [10]. Moreover, doped additives, such as metals and metal oxides, promotes gas sensitivity or lower the working temperature [2, 11]. Particularly, Pd⁰ or PdO is frequently doped on SnO₂ particles because PdO acts as a strong acceptor of electrons and also extracts electrons from the oxide. Yanbai Shen and others reported that noble metals (Pd, Pt, etc.) on the surface of SnO₂ worked as catalysts, which not only created enhanced sites for gas molecular adsorption, but also lowered the activation energy required for the sensing reaction to take place [12–14].

Carbon monoxide (CO) is one of most poisonous gases. When exposed to high concentrations, humans and other

animals can suffer from CO poisoning. Symptoms include headaches, nausea, shortness of breath, dizziness, and fatigue some of which may even occur exposed to low concentrations [15–18]. Thus, a CO gas sensor is urgently needed. Table 1 lists the responses of some typical semiconductor oxide based CO gas sensors. We had previously concluded that a low optimized operating temperature and a high sensitivity did not occur concurrently in the sensors, so finding a low temperature CO gas sensor with high sensitivity was extremely desirable [19–25]. Carbon nanotubes (CNTs) as one of the ideal materials for gas sensors have attracted extensive attention due to their unique physical, chemical and electrical properties [26–28]. Most importantly, the decoration of CNTs with metal or metal oxide nanoparticles has also been exploited to improve gas sensing performance [29, 30].

In this study, a sol-gel method was used to synthesize a CNT that was coated by Pd²⁺-doped SnO₂ (Pd²⁺/SnO₂/CNT) nanocomposites to prepare a CO gas sensor. The optimal Pd²⁺ doping concentration for better gas-sensing property was 1.0 mol% and the optimal CNT/Sn molar ratio is 0.12. The sensor response is up to 104 upon exposure to 500 ppm CO at the working temperature of 100 °C, and the stability of the nanocomposites was also very good.

2 Experimental

2.1 Materials and preparation of Pd²⁺/SnO₂/CNT nanocomposites

Tin (IV) chloride penta-hydrate (SnCl₄·5H₂O) was obtained from Nanjing Chemical Reagent Co., Ltd. Urea and Citric acid monohydrate were purchased from Sinopharm Chemical Reagent Co., Ltd. Ammonia (NH₃·H₂O) was got from Xilong Chemical Co., Ltd. Palladium (II) chloride acid sodium (Na₂PdCl₄) was obtained from Sinopharm Chemical Reagent Co., Ltd. The single-walled CNTs were purchased from Shenzhen Nanotech Port Co., Ltd. We used ultrapure water (with a resistivity is of 18.05 MΩcm⁻¹) in this work.

To increase the surface functional groups, pretreatment was needed for the CNT. We heated the CNT in HNO₃ under reflux for 12 h at 80 °C, then rinsed and dried them at 80 °C for 4 h.

Pd²⁺/SnO₂/CNT nanocomposites were synthesized by a sol-gel method. SnCl₄·5H₂O (0.1 M) and citric acid monohydrate (the mole ratio citric acid: SnCl₄·5H₂O was

equal 1:15) were dissolved into 100 mL ultrapure water under magnetic stirring for 10 min. We then added the solution to the suspension of CNT (the molar ratio CNT: SnCl₄·5H₂O was equal 0.06, 0.12, 0.24, 0.48, respectively) under ultrasonic for 30 min. Subsequently, we added the aqueous solution of urea (the mole ratio of Sn⁴⁺: urea was 1:20) to the above solution under magnetic stirring at 90 °C for 30 min. The dopant of Na₂PdCl₄ solution was added slowly into the above suspension under magnetic stirring at 90 °C. Then, the ammonia solution was added to adjust the pH level to approximately 8–9 and the precursor suspension was stirred at 90 °C for 4 h. The gel was washed and centrifugalized with ultrapure water and ethanol at least three times and subsequently dried in a vacuum oven at 80 °C for 4 h. Finally, the resulting solid was annealed in a furnace at 500 °C for 4 h. The dopant concentrations in the mole fabrication of the Pd²⁺ were set as 0, 0.5, 1.0, 3.0, and 5.0 mol%, respectively.

2.2 Fabrication and measurement of CO gas sensor based on our products

The sensor device was composed of alumina substrates equipped with a pair of comb-type Au interdigitated electrodes, which were obtained from SiPing, Jilin China High-Tech Co., Ltd. The nanocomposites were mixed with ultrapure water to form a paste, which was then coated on the surface of the sensor device (Fig. 1a), and later dried in the shade to form a gas sensor, as shown in Fig. 1b.

We measured the gas sensing properties using the CGS-1TP intelligent test system (Beijing Elite Tech Co. Ltd., China). When the resistance of the sensor was stable, the saturated target gas was injected into the test chamber (18 L in volume) by inserting a microsyringe through a rubber plug. After reaching a new constant value, the test chamber was opened until the resistance of the sensor returned to its original situation. All of the measurements were performed in a laboratory fume hood. The sensor resistance and response values were automatically acquired from by the analysis system. R_a is the resistance of the sensor in the air and R_g is the resistance of the sensor in test gas. The sensor response was defined as the ratio R_a/R_g . The time taken by the sensor to achieve 90% of the total resistance change was defined as the response time in the case of adsorption or the recovery time in the case of desorption.

Table 1 The response of some typical semiconductor oxide based CO sensors.

materials	temperature	sensitivity	response	ref.
SnO ₂ nanobelt	400 °C	7 (250 ppm)	~30 s	[19]
NiO nanowire	150 °C	0.25 (800 ppm)	~2 h	[20]
CeO ₂ nanowire	25 °C	2 (200 ppm)	~10 s	[21]
TiO ₂ nanofiber	300 °C	21 (100 ppm)	~4 s	[22]
ZnO nanowire	300 °C	82 (300 ppm)	–	[23]
ZnO/SnO ₂	300 °C	2.5 (320 ppm)	–	[24]
Sn _{1-x} Ce _x O _{2-d}	300 °C	2.5 (320 ppm)	–	[25]
Pd ²⁺ /SnO ₂ /CNT	100 °C	104 (500 ppm)	~2 s	this work

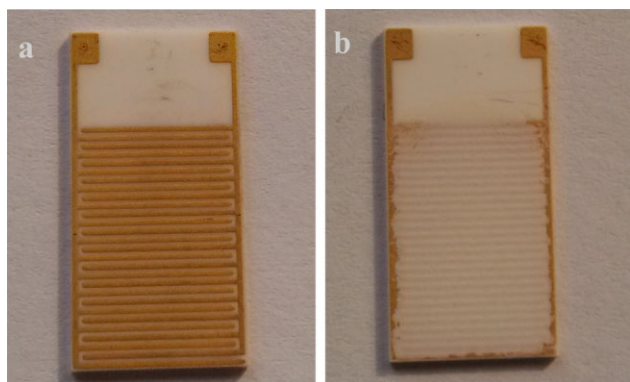


Figure 1 (a) Sensor device, (b) coated sample.

2.3 Characterization The nanocomposites were characterized via X-ray diffraction (XRD, Bruker AXS D8, advance diffractometer with a $\text{Cu K}\alpha$ $\lambda = 1.540562 \text{ \AA}$ radiation). We then used transmission electron micrographs (TEM, Philips CM12) to obtain the morphology. A VG Multilab 2000 \times (VG Co.) spectrometer was utilized to perform a XPS analysis of the hybrid $\text{Pd}^{2+}/\text{SnO}_2/\text{CNT}$. An $\text{Al K}\alpha$ X-ray source was used, with the anode operating at 9 kV and 18.5 mA.

3 Results and discussion

3.1 XRD Figure 2 presents the XRD patterns for the 1.0 mol% Pd^{2+} doping $\text{Pd}^{2+}/\text{SnO}_2/\text{CNT}$ nanocomposites with a CNT/Sn molar ratio range from 0.06 to 0.48, while CNT/Sn = 0.0 represents 1.0 mol% $\text{Pd}^{2+}/\text{SnO}_2$. All of the patterns displayed clear reflections at certain degrees, ranging from (110), (101) to (211) etc. All of the peaks were perfectly indexed to the tetragonal rutile SnO_2 structure (JCPDS File No. 41-1445), with lattice constants of $a = 4.738 \text{ \AA}$ and $c = 3.187 \text{ \AA}$, which are in agreement with other reports [31]. The FWHM of the diffraction peaks increased, which indicated that the grain size rapidly

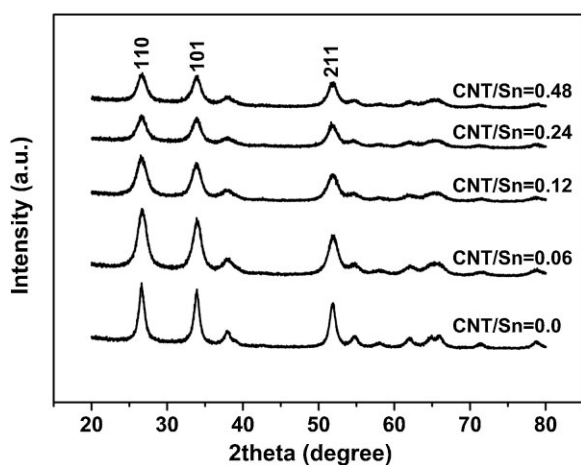


Figure 2 XRD patterns of $\text{Pd}^{2+}/\text{SnO}_2/\text{CNT}$ and $\text{Pd}^{2+}/\text{SnO}_2$ nanocomposites.

decreased as the concentration of the CNT concentration increased. There are no diffraction peaks of PdO in the patterns, which may be due to low amounts of Pd^{2+} loaded in the SnO_2 or a homogeneous distribution of Pd^{2+} doping [32]. Furthermore, it is hard to elicit the characteristic peaks of CNTs from XRD patterns because of the overlap of SnO_2 (110) and (211) peaks with the peaks of CNTs at diffraction angle $2\theta = 26.70^\circ$ and at 51.51° [30].

3.2 TEM The morphology of the samples was observed by means of TEM. Figure 3a shows the TEM images of pristine CNTs. Figures 3b and c demonstrate the TEM images of the prepared 1.0 mol% $\text{Pd}^{2+}/\text{SnO}_2$, and the sample of 1.0 mol% $\text{Pd}^{2+}/\text{SnO}_2/\text{CNT}$ (CNT/Sn = 0.12), respectively. Electron microscopy analyses reveal that the Pd^{2+} -doped SnO_2 nanoparticles with diameters in the range of 8–20 nm formed massive aggregates; however, when loaded in the CNT, the $\text{Pd}^{2+}/\text{SnO}_2$ grains were dispersed on the nanotubes surface. We speculated that the CNTs prevent SnO_2 particles from forming massive agglomerations, because of the fact that the SnO_2 particles likely anchored on the hydroxyl and carboxylic groups that were introduced during the CNT surface functionalization. Figure 3d shows the HR-TEM image of the sample of the $\text{Pd}^{2+}/\text{SnO}_2/\text{CNT}$. The lattice spacing measurements of the nanocomposites give recurrent values of 0.33 and 0.26 nm, which is corresponding to the rutile SnO_2 (110) and (101) plane, respectively. The interplanar spacing of 0.19 nm corresponds to the PdO (200) plane.

3.3 XPS The chemical composition of the specimens after calcinations and in situ reduction was examined by X-ray photoelectron spectroscopy (XPS). The binding

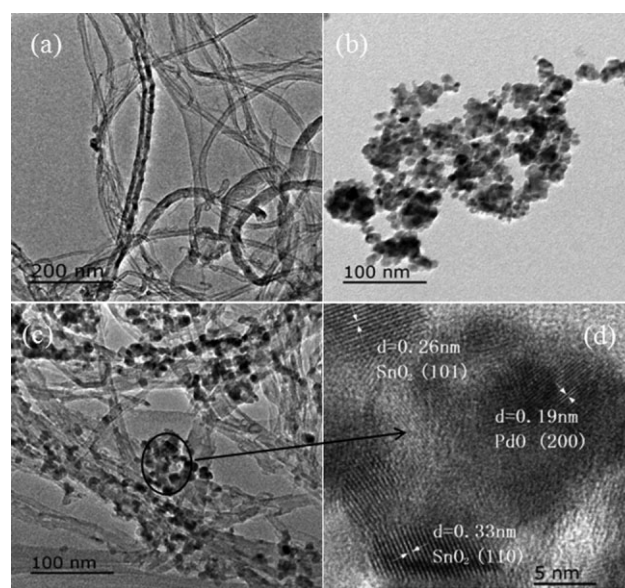


Figure 3 TEM images of (a) CNTs; (b) 1.0 mol% $\text{Pd}^{2+}/\text{SnO}_2$; (c) 1.0 mol% $\text{Pd}^{2+}/\text{SnO}_2/\text{CNT}$ (CNT/Sn = 0.12); and (d) HR-TEM of the $\text{Pd}^{2+}/\text{SnO}_2/\text{CNT}$ nanocomposites.

energies were calibrated using a reference of C 1s at 284.8 eV for adventitious hydrocarbon contamination [33]. Figure 4 shows the Sn 3d and Pd 3d of photoemission spectra of Pd²⁺/SnO₂ specimen before and after in situ reduction. In Fig. 4a, we can clearly see the Sn 3d doublet characterized by 3d_{3/2}-3d_{5/2} splitting. In situ reduction in hydrazine hydrate did not produce any significant reduction of Sn⁴⁺ as detected by XPS. In terms of Pd 3d, the characteristic peak of Pd 3d_{5/2} with a binding energy of 337.1 eV corresponds to Pd²⁺ (PdO); after in situ reduction, the peak shifts to a binding energy of 335.05 eV assigned to a Pd⁰ peak, as shown in Fig. 4b.

3.4 CO sensing test To examine the effects of Pd²⁺ doping and CNT-loading on sensor properties, we fabricated gas sensors that were comprised of different Pd²⁺ loading levels, with a CNT/Sn molar ratio range from 0.06 to 0.48, and measured their resistance response. The optimum working temperature range is an important functional characteristic for semiconductor oxide sensors. Figure 5a shows the sensors' response to 500 ppm CO with different Pd²⁺ loading levels from 0.0 mol% to 5.0 mol% and a

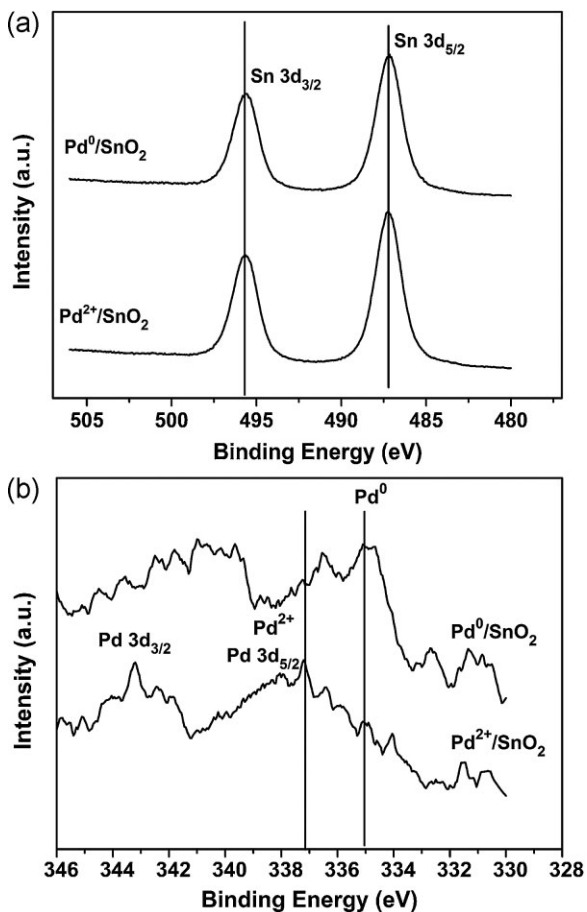


Figure 4 XPS spectra of (a) the Sn 3d and (b) the Pd 3d with sensitive materials before (Pd²⁺/SnO₂) and after in situ reduction (Pd⁰/SnO₂).

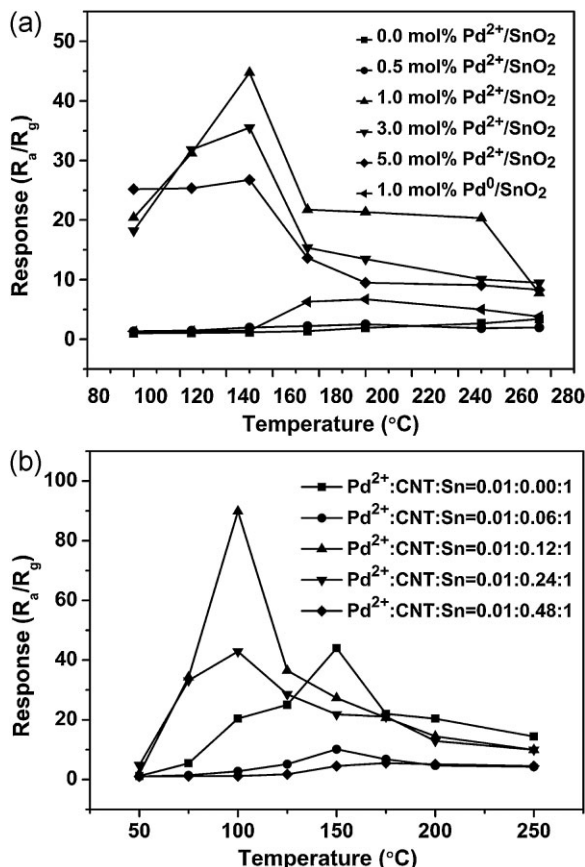


Figure 5 (a) Response to CO of the Pd²⁺/SnO₂ sensors with different Pd²⁺-loading levels at different operating temperatures. (b) Response to CO of the Pd²⁺/SnO₂/CNT sensor with 1.0 mol% Pd²⁺-doped SnO₂ sensors at different operating temperatures.

1.0 mol% Pd²⁺/SnO₂ in situ reduction in hydrazine hydrate at operating temperatures ranging from 100 °C to 275 °C. We observed that the sensor-doped Pd²⁺ has a great influence on the sensor's response. The best performance of Pd²⁺/SnO₂ sensors is observed for 1.0 mol% Pd²⁺/SnO₂ as active layer. The maximum response to 500 ppm CO is 38 times higher than pure SnO₂ at 150 °C. After in situ reduction in hydrazine hydrate, the response to CO decreased, as compared to 1.0 mol% Pd²⁺/SnO₂ materials, which implies that Pd²⁺ is the key to promoting sensitivity. Figure 5b demonstrates the response of the CNT coated with Pd²⁺-doped SnO₂ nanoparticles to 500 ppm CO with different CNT/Sn molar ratios and a Pd²⁺ concentration of 1.0 mol%. The hybrid Pd²⁺/SnO₂/CNT sensors exhibit a high sensitivity and a low optimum working temperature when the CNT/Sn molar ratio is 0.12. The sensitivity of the materials improved to 80 times higher than pure tin oxide at a CO concentration of 500 ppm. For the Pd²⁺/SnO₂/CNT nanoparticles, the optimum operating temperatures significantly decreased and the sensitivity rapidly increased by loading Pd²⁺ and

CNT, which clearly indicates the beneficial effects of Pd^{2+} and CNT-loading.

Figure 6a shows the variations of the sensor's sensitivity and response–recovery time, when measured at 150°C based on $1.0\text{ mol}\% \text{Pd}^{2+}/\text{SnO}_2$, owing to its exposure to carbon monoxide. We explored a wide range of CO concentration from 10 ppm to 1000 ppm of CO concentration. Notably, the $1.0\text{ mol}\% \text{Pd}^{2+}/\text{SnO}_2$ sensor had a short response (5–20 s) and corresponding recovery (25–45 s) time. As seen in the

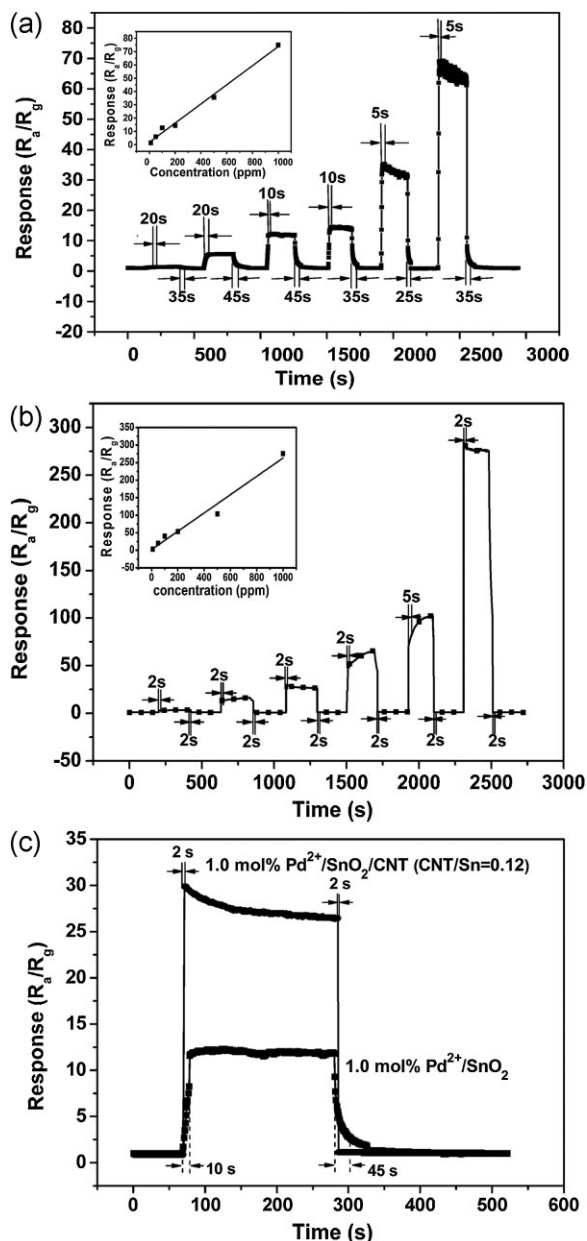


Figure 6 (a) Dynamic CO sensing transients of the sensor with $1.0\text{ mol}\% \text{Pd}^{2+}/\text{SnO}_2$ as active layer at 150°C to 10, 50, 100, 200, 500, 1000 ppm, respectively, illustrating the relationship between CO concentration and sensitivity. (b) The sensor of $1.0\text{ mol}\% \text{Pd}^{2+}/\text{SnO}_2/\text{CNT}$ (CNT/Sn=0.12) at 100°C . (c) Response curves to 100 ppm CO of the sensors.

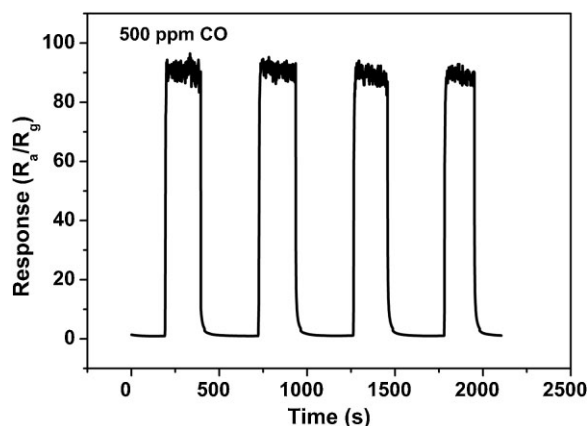


Figure 7 Stability of the $1.0\text{ mol}\% \text{Pd}^{2+}/\text{SnO}_2/\text{CNT}$ (CNT/Sn=0.12) sensor against 500 ppm CO at 100°C .

illustrations (inset in Fig. 6a and b), a linear correlation occurred between sensitivity and the CO concentration. It should be indicated that, for gas sensor application, the concentration of CO widely varies. When comparing $1.0\text{ mol}\% \text{Pd}^{2+}/\text{SnO}_2/\text{CNT}$ (CNT/Sn=0.12) sensor to $1.0\text{ mol}\% \text{Pd}/\text{SnO}_2$ sensor, the former sensor adding CNT demonstrates a much faster response–recovery time ($t_{90} \leq 2\text{ s}$) to CO at 100°C , as shown in Fig. 6c CNT likely plays a significant role in the low response–recovery time of the composite sensors.

Stability is one of the important parameters of the sensor. Figure 7 shows the stability of the sensor whose active layer was comprised of $1.0\text{ mol}\% \text{Pd}^{2+}$ doping and with a CNT/Sn molar ratio of 0.12 $\text{Pd}^{2+}/\text{SnO}_2/\text{CNT}$ against 500 ppm of CO at 100°C . Four periods were examined, the standard deviation of which was approximately 0.26%. This suggests that high repeatability and stability were achieved.

A well-defined ability to detect a target gas is important toward good fundamental for a real-time gas sensing device. The sensitivity values of $0.0\text{ mol}\% \text{Pd}^{2+}/\text{SnO}_2$, $1.0\text{ mol}\%$

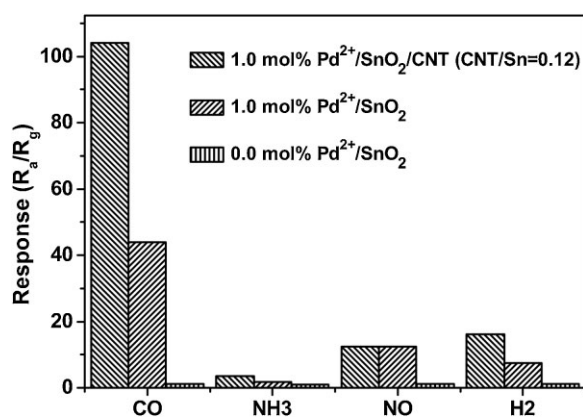


Figure 8 Response to different gases of the $0.0\text{ mol}\% \text{Pd}^{2+}/\text{SnO}_2$, $1.0\text{ mol}\% \text{Pd}^{2+}/\text{SnO}_2$, and $1.0\text{ mol}\% \text{Pd}^{2+}/\text{SnO}_2/\text{CNT}$ (CNT/Sn=0.12) sensors against 500 ppm CO at 100°C .

$\text{Pd}^{2+}/\text{SnO}_2$, and 1.0 mol% $\text{Pd}^{2+}/\text{SnO}_2/\text{CNT}$ ($\text{CNT}/\text{Sn} = 0.12$) to various gases (CO , NH_3 , H_2 , NO) at 500 ppm were measured, as shown in Figure 8. As indicated, the sensor of 1.0 mol% $\text{Pd}^{2+}/\text{SnO}_2/\text{CNT}$ ($\text{CNT}/\text{Sn} = 0.12$) exhibited better selectivity, because it has higher sensitivity to CO in presence of NH_3 , H_2 , and NO . Therefore, it is concluded that Pd^{2+} doping is the key to promoting the sensor sensitivity, while CNT adding to $\text{Pd}^{2+}/\text{SnO}_2$ can decrease response–recovery time, and improve stability as well as selectivity.

4 Conclusions In summary, we synthesized the hybrid $\text{Pd}^{2+}/\text{SnO}_2/\text{CNT}$ using a sol–gel method, which consisted of different Pd-loaded levels and CNT-doped levels, in order to thoroughly investigate the carbon monoxide sensors. The results revealed that a 1.0 mol % Pd^{2+} doping SnO_2 with CNT/Sn molar ratio of 0.12 exhibited high sensitivity, selectivity, repeatability, a low limit of detection (5 ppm, $R_a/R_g = 1.95$), and a fast response–recovery time ($t_{90} \leq 2$ s) to CO at 100 °C. The characterization studies show that the CNTs prevent the SnO_2 particles from forming massive agglomerations, because the SnO_2 particles likely anchored to the hydroxyl and carboxylic groups introduced during CNT surface functionalization. This introduction likely decreased the response–recovery time. In order to explain the chemical state of Pd^{2+} on sensing performance, a in situ reduction was formulated; the results indicated that Pd^{2+} doping is the key to promoting sensitivity.

Acknowledgements This work was financially supported by the National Natural Science Foundation of China (No. 20873097, 21071113), Natural Science Foundation of Hubei Province (No. 2011CDA049), International Cooperation Foundation of Hubei Province (2012IHA00201).

References

- [1] G. H. Lu, L. E. Ocola, and J. H. Chen, *Adv. Mater.* **21**, 2487 (2009).
- [2] M. Yuasa, T. Kida, and K. Shimano, *Appl. Mater. Interf.* **4**, 4231 (2012).
- [3] E. Nikan, A. A. Khodadadi, and Y. Mortazavi, *Sens. Actuators B* **184**, 196 (2013).
- [4] M. Batzill and U. Diebold, *Prog. Surf. Sci.* **79**, 147 (2005).
- [5] S. Habibzadeh, A. A. Khodadadi, and Y. Mortazavi, *Sens. Actuators B* **144**, 131 (2010).
- [6] O. Lupan, L. Chow, G. Chai, H. Heinrich, S. Park, and A. Schulte, *Physica E* **41**, 533 (2009).
- [7] P. S. Patil, S. B. Sadale, S. H. Mujawar, P. S. Shinde, and P. S. Chigare, *Appl. Surf. Sci.* **253**, 8560 (2007).
- [8] Y. Matsui, M. Mitsuhashi, and Y. Goto, *Surf. Coat. Technol.* **169-170**, 549 (2003).
- [9] J. Mazloom, F. E. Ghodsi, and M. Gholami, *J. Alloys Compd.* **579**, 384 (2013).
- [10] M. M. Arafat, B. Dinan, S. A. Akbar, and A. S. M. A. Haseeb, *Sensors* **12**, 7207 (2012).
- [11] A. Khodadadi, S. S. Mohajerzadeh, Y. Mortazavi, and A. M. Miri, *Sens. Actuators B* **80**, 267 (2001).
- [12] Y. Shen, T. Yamazaki, Z. Liu, D. Meng, and T. Kikuta, *Thin Solid Films* **517**, 6119 (2009).
- [13] Y. I. Lee, K. J. Lee, D. H. Lee, Y. K. Jeong, H. S. Lee, and Y. H. Choa, *Curr. Appl. Phys.* **9**, S79 (2009).
- [14] L. K. Bagal, J. Y. Patil, I. S. Mulla, and S. S. Suryavanshi, *Ceram. Int.* **38**, 4835 (2012).
- [15] L. De Luca, A. Donato, S. Santangelo, G. Faggio, G. Messina, N. Donato, and G. Neri, *Int. J. Hydrogen Energy* **37**, 1842 (2012).
- [16] J. Y. Choi and T. S. Oh, *Thin Solid Films* **547**, 230–2234 (2013).
- [17] B. Bahrami, A. Khodadadi, M. Kazemeini, and Y. Mortazavi, *Sens. Actuators B* **133**, 352 (2008).
- [18] L. Madler, T. Sahm, A. Gurlo, J. D. Grunwaldt, N. Barsan, U. Weimar, and S. E. Pratsinis, *J. Nanopart. Res.* **8**, 783 (2006).
- [19] L. H. Qian, K. Wang, Y. Li, H. T. Fang, Q. H. Lu, and X. L. Ma, *Mater. Chem. Phys.* **10**, 82 (2006).
- [20] J. S. Tresback and N. P. Padture, *J. Mater. Res.* **23**, 2047 (2008).
- [21] L. Liao, H. X. Mai, Q. Yuan, H. B. Lu, J. C. Li, C. Liu, C. H. Yan, Z. X. Shen, and T. Yu, *J. Phys. Chem. C* **112**, 9061 (2008).
- [22] W. Biao, Z. Y. Dong, H. L. Ming, C. J. Sheng, G. F. Li, L. Yun, and W. L. Jun, *Chin. Sci. Bull.* **55**, 228 (2010).
- [23] T. J. Hsueh, Y. W. Chen, S. J. Chang, S. F. Wang, C. L. Hsu, Y. R. Lin, T. S. Lin, and I. C. Chen, *Sens. Actuators B* **125**, 498 (2007).
- [24] E. Nikan, A. A. Khodadadi, and Y. Mortazavi, *Sens. Actuators B* **184**, 196 (2013).
- [25] S. Somacescu, P. Osiceanu, J. M. C. Moreno, L. Navarrete, and J. M. Serra, *Microporous Mesoporous Mater.* **179**, 78 (2013).
- [26] E. Llobet, *Sens. Actuators, B* **179**, 32 (2013).
- [27] K. H. An, S. Y. Jeong, H. R. Hwang, and Y. H. Lee, *Adv. Mater.* **16**, 1005 (2004).
- [28] D. Zhang, K. Wang, J. Tong, and B. Xia, *Microsyst. Technol.* **20**, 379 (2014).
- [29] Z. K. Horastani, S. M. Sayedi, and M. H. Sheikhi, *Sens. Actuators B* **202**, 461 (2014).
- [30] V. M. Aroutiounian, A. Z. Adamyan, E. A. Khachatryan, Z. N. Adamyan, K. Hernadi, Z. Pallai, Z. Nemeth, L. Forro, A. Magrez, and E. Horvath, *Sens. Actuators B* **177**, 308 (2013).
- [31] H. Kim, C. Jin, S. Park, and C. Lee, *Mater. Res. Bull.* **47**, 2708 (2012).
- [32] J. Zhao, W. Wang, Y. Liu, J. Ma, X. Li, Y. Du, and G. Lu, *Sens. Actuators B* **160**, 604 (2011).
- [33] X. Y. Du, Y. Wang, Y. Y. Mu, L. I. Gui, P. Wang, and Y. Q. Tang, *J. Chem. Mater.* **14**, 3953 (2002).